Collapse displacements of masonry arch with geometrical uncertainties on spreading supports

P. Zampieri, N. Cavalagli*, V. Gusella, C. Pellegrino

This work is aimed at evaluating the collapse displacement of masonry arch subjected to spreading supports. This is achieved through a general application of the virtual works principle. The problem is described in a finite displacements formulation and investigated with a probabilistic approach, also considering the effects of the geometrical uncertainties. This aspect is related to the imperfections of the voussoirs, which affect the structural shape. The comparison between the numerical and experimental results, derived both by the literature and laboratory tests, confirms that the geometrical irregularities can significantly affect the results obtained on the nominal structural geometry. Moreover, the disagreement observed in the experimental tests is explained.

Keywords: masonry arch; spreading support; irregular geometry; uncertainties; limit equilibrium

1. Introduction

The masonry arch is one of the most commonly used structural components in the historical constructions. In the last centuries, the understanding of its behaviour has received a growing interest of architects, engineers and researchers, especially for the development of the scientific method. As for the more general cases of vaulted systems, the main function of a masonry arch is to bring the upper loads through specific ways of the structure to the ground, covering small or large spaces. The definition of the bearing capacity is a crucial task for the right dimensioning of an arch. In the case of restoration and/or retrofitting of existing buildings, bearing capacity is also fundamental for its check and validation. In the last decades, the scientific literature on this topic has considerably grown and the level of knowledge has significantly increased. In the

The published version of the paper "P. Zampieri, N. Cavalagli, V. Gusella, C. Pellegrino, Collapse displacements of masonry arch with geometrical uncertainties on spreading supports, Computers & Structures, Volume 208, 2018, Pages 118-129, ISSN 0045-7949" is available at: https://doi.org/10.1016/j.compstruc.2018.07.001

second half of the XX century, a fundamental contribution was provided by Heyman [1,2], who used limit analysis for the study of masonry structures with an efficient approach for the rapid evaluation of the structural limit conditions. In this work, conceivable simplified hypotheses were assumed: no-tensile material, infinite compressive strength and no-sliding condition at failure between the voussoirs. The method is based on the well-known safe theorem, which states that “if a set of internal forces in a masonry structure can be found that equilibrate the external loads, and which lie everywhere within the masonry, then the structure is safe – safe in the sense that it cannot collapse under those loads” [3]. After Heyman’s model, the upper bound and the lower bound methods or, alternatively, the limit equilibrium state analysis have been largely used. These methods were applied with several purposes, as the definition of the minimum thickness and/or the bearing capacity under vertical and lateral loads for different shapes of arches [4-11], the study of arches and vaults behaviour by using the thrust network analysis [12-15] or advanced numerical methods [16-19], the analysis of the strengthening effects through innovative materials [20-25] and many others.

During its life, a masonry arch has to withstand several threats that could significantly reduce its bearing capacity. This problem can be mainly related to two aspects: (i) structural damages of the arch (e.g. openings or sliding between the voussoirs due to load actions) and/or material degradation (reduction of the arch thickness or the strength of materials); (ii) springing settlements.

As far as it concerns the evaluation of structural and material degradation effects, in the last years several works have been focused on the assessment of the strength or stability reduction of a masonry arch due to its irregular geometry. The problem was investigated by modelling masonry arches taking into account the actual stones dimensions [26,27]. Elsewhere, parametric studies were applied to investigate the influence of localized damages [28,29] or probabilistic approaches were used for the estimation of uncertainties effects on the bearing structural capacity considering horizontal loads, both in static [30] and dynamic conditions [31]. These works emphasized that in the most cases the reduction of the collapse conditions, with respect to the results obtained on the structures having nominal geometries, cannot be neglected.

Regarding the study of the springing settlements effects, it can be stated that some aspects concerning the structural response of masonry arches – and more in general of masonry vaults – still present open problems. Differential settlements can be considered one of the main causes of collapse of vaulted structures [4], occurring for slow long-term deformations, for example due to static loads, or very quickly dynamic behaviour of the building, as in the case of earthquake actions. In a study concerning settled pushing structures, in particular arches and domes, Como [32] demonstrated "that, if the geometry changes are negligible, the structure will attain the minimum thrust state, saving its safety margin as in the perfect state". Ochsendorf [33] analysed the collapse conditions of the masonry arch on spreading supports in horizontal direction as a function of the geometrical parameters, namely the curvature radius, the thickness and the angle of embrace. Experimental results pointed out that the hinges may move with the increase of the settlements before reaching the collapse. Galassi *et al.* [34] studied the response of masonry structures to settlements considering rigid blocks connected by unilateral contact and frictional links, through a non-linear numerical procedure experimentally validated. Starting from the work of Ochsendorf, Coccia *et al.* [35] developed an incremental procedure, based on the kinematic theorem applied to the deformed configuration. They aimed at attaining the collapse conditions of the masonry arch with horizontal spreading supports by varying the geometrical parameters and the number of voussoirs. Zang *et al*. [36] analysed the masonry arch on spreading supports through a mesoscale modelling strategy, considering solid elements for bricks connected by interface elements for mortar joints. Constitutive models allow to consider the effects related to the possible presence of damages. Recently, Zampieri *et al.* analysed the effects of local pier scour in a multi-span masonry bridges [37] and the influence of no-horizontal springing supports of the masonry arch on the collapse mechanisms, with a numerical approach supported by experimental observations [38,39].

As pointed out by literature works, numerical simulations carried out on nominal geometry models seem to overestimate experimental results [4,33,35]. Starting from this point, this paper is aimed at investigating the role of geometrical irregularities, evaluated through a probabilistic approach, on the collapse conditions of a masonry arch subjected to spreading supports, which could be also related to abutments or piers deformations. In particular, the collapse conditions are studied through an incremental numerical procedure using the virtual works principle applied at the deformed configuration. For each deformed configuration, the limit equilibrium approach is used to assure the structural equilibrium and the strength condition defining the right hinges configurations. This condition occurs when the thrust line is contained inside the arch and passes through the hinge points.

Considering two experimental tests, in this work it is demonstrated for the first time that the reduction of the ultimate displacement observed at collapse, can be related to geometrical uncertainties, if compared with numerical simulations. This aspect leads to the opportunity of introducing safety factors in order to take into account such effects also in engineering practice [30].

2. Problem statement and numerical procedure

2.1 Basic hypotheses

Let us consider a circular masonry arch of radius r, thickness t and angle of embrace α made by n voussoirs under only its own weight in equilibrium state (Figure 1). The generic ith voussoir is subjected to the vertical force

$$g_i = \gamma A_i d \qquad (1)$$

where γ is the specific weight, A_i the area of the ith voussoir and d the constant out-of-plane depth. The arch is supposed to be fixed on a spreading support, in particular the left support without loss of generality (point $P_0(x_0, y_0)$ in Figure 2), and the direction of the settlement δ_0 identified by the angle θ with respect to the horizontal. Given the geometrical parameters, the Cartesian coordinates of a generic point belonging to the arch can be indicated as a function of the radius r, thickness t and angle of embrace α. As an example, with reference to the *Oxy* system indicated in Figure 1, the coordinates of the centre of mass of the ith voussoir are

$$x_i = r\cos\beta - r\cos\left(\beta + \frac{\alpha_i}{2} + (i-1)\alpha_i\right) \qquad (2)$$

$$y_i = -r\sin\beta + r\sin\left(\beta + \frac{\alpha_i}{2} + (i-1)\alpha_i\right) \qquad (3)$$

being $\beta = (\pi - \alpha)/2$ and $\alpha_i = \alpha / n$.

The passage form the initial unsettled configuration Ω^0 to an equilibrated settled configuration Ω^k induced by the spreading support is described by a kinematic mechanism consisting of a three-hinged rigid body chain.

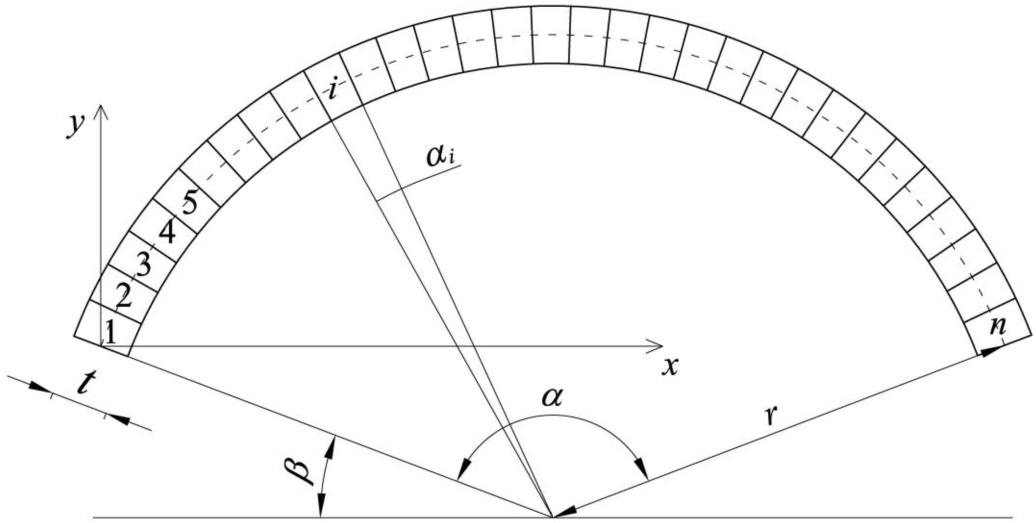

Figure 1. Illustration of a masonry arch, divided in *n* voussoirs, with its geometrical parameters: radius *r*, thickness *t* and angle of embrace *α*.

The mechanism can be analysed with the well-known hypotheses proposed by Heyman [1]: (i) mechanism condition, (ii) resistance criterion and (iii) equilibrium condition. The first condition (i) requires that the mechanism is only of rotational type, so that no sliding can occur at each joint; the second (ii) considers a material with infinite compressive strength and no-tensile strength; the third (iii) corresponds to the individuation of a thrust line – equilibrated with the external loads – everywhere contained inside the arch parts profile and passing through the hinges. The ultimate state of equilibrium is reached by progressively increasing the value of the displacement δ_0 up to the loss of stability of the arch. This condition leads to the structural collapse with a mechanism which may involve either all the voussoirs, with a five-hinges symmetric mechanism, or a part of them, with the occurrence of an asymmetric configuration. In this case the collapse may develop starting from a four-hinges mechanism, or due to the alignment of the three hinges already present (three-hinges mechanism).

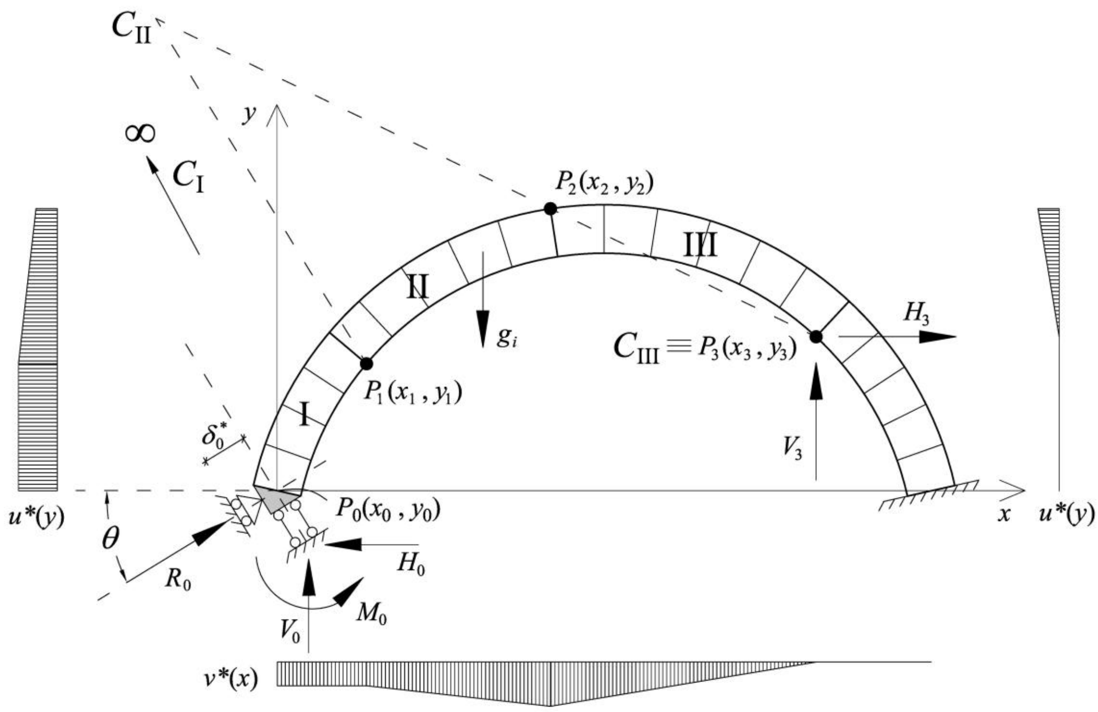

Figure 2. Virtual displacement diagrams applied to the masonry arch for the determination of the reaction force R_0.

Let us consider the settlement δ_0 assigned in P_0 along θ direction and the resulting kinematically admissible displacement field $\delta(u,v)$ of the structure, with u and v as displacement components in x and y directions respectively. The equation of the virtual works – employed in the small displacement field – provided by the equilibrated settled configuration Ω^k and a virtual displacement field δ^{k*} having the same properties previously described (i.e. δ_0^{k*} defined in θ direction and δ^{k*} kinematically admissible) is

$$\left\langle g,\delta^{k*}\right\rangle + R_0^k \cdot \delta_0^{k*} = \left\langle \sigma^k,\varepsilon^{k*}\right\rangle \tag{4}$$

where σ^k and ε^{k*} are the stress and strain fields respectively, and R_0^k is the reaction force acting on P_0 along θ direction. In the Equation (4), the notation $\langle \bullet,\circ \rangle$ indicates the work calculus given by the system "$\bullet$" of forces or stresses, and the system "$\circ$" of displacements or strains [40]. Assuming that the elastic deformations can be considered everywhere negligible, the right side of Equation (4) vanishes

$$\left\langle \sigma, \varepsilon^{k*} \right\rangle = 0 \tag{5}$$

so that it is possible to calculate the reaction force along the settlement direction

$$R_0^k = -\frac{\left\langle g, \delta^{k*} \right\rangle}{\delta_0^{k*}} \tag{6}$$

Following the notation of Figure 2, the solution of the equilibrium problem is easily given by a system of equilibrium equations (three global equilibrium conditions and a balance equation around the point P_2) expressed in the matrix form [37]

$$\mathbf{Q} \cdot \mathbf{r} = \mathbf{q} \tag{7}$$

where **Q** is the coefficient matrix

$$\mathbf{Q} = \begin{bmatrix} 1 & 0 & 1 & 0 \\ -\tan\theta & 0 & 0 & 1 \\ 0 & -1 & (x_0 - x_3) & (y_3 - y_0) \\ 0 & 0 & (x_2 - x_3) & (y_3 - y_2) \end{bmatrix} \tag{8}$$

r is the vector of the unknown reaction forces

$$\mathbf{r} = \begin{Bmatrix} V_0 \\ M_0 \\ V_3 \\ H_3 \end{Bmatrix} \tag{9}$$

and **q** is the vector of the known terms

$$\mathbf{q} = \begin{Bmatrix} F_{03} - R_{0V}^k \\ -R_{0H}^k \\ -F_{03} b_{03} \\ -F_{23} b_{23} \end{Bmatrix} \tag{10}$$

in which F_{03} and F_{23} are the resultant vertical forces of the structural parts comprised between the points $P_0 - P_3$ and $P_2 - P_3$ respectively, $R_{0V}^k = R_0^k \sin\theta$ and $R_{0H}^k = R_0^k \cos\theta$

are the vertical and horizontal components of the reaction R_0^k, while b_{03} is the distance between P_0 and the line of action of F_{03}, and b_{23} between P_3 and the line of action of F_{23}.

The problem solution is achieved through the following equation

$$\mathbf{r} = \mathbf{Q}^{-1} \cdot \mathbf{q} \tag{11}$$

from which the horizontal component H_0 is derived through the relation $H_0 = V_0 \tan\theta$. If Heyman hypothesis about the criterion resistance is satisfied, namely the thrust line is everywhere inside the arch profile in each block, the solution is admissible, otherwise the hinges must be moved and the solution is achieved by means of few iterations.

As discussed above, the collapse condition can be reached for the arising of several types of mechanisms. Several authors asserted that the type of collapse mechanism depends on several features, in particular the arch geometry (e.g. the rise, the span and the thickness) and the settlement direction [4,33,35]. It is well-known from the literature that a three hinges mechanism suddenly develop with an even small settlement and then, with the increasing of the displacement, evolves up to the arch collapse. During this process, it is also possible to observe a change of mechanism, characterized by a movement of the hinges before the collapse.

In this perspective, the description of the mechanism evolution requires a finite displacements formulation of the problem, in order to define the geometrical configuration of the kinematic structural mechanism, also considering the possible change of the hinges position, until reaching collapse.

2.2 Numerical procedure in finite displacement field

The structural problem introduced in the previous section, regarding the research of the ultimate condition of an arch subjected to a spreading support, is solved through an incremental numerical procedure based on increasing values of the assigned settlement. The search algorithm of the ultimate condition, developed in the finite displacements field, consists of three main steps.

The first step is dedicated to the identification of the kinematic mechanism corresponding to the initial unsettled configuration Ω^0 (Figure 2). Through an iterative procedure, it is possible to identify a virtual displacement field δ^{0*} associated to a kinematically admissible mechanism. The procedure, based on the three Heyman hypotheses previously recalled, allows to obtain an equilibrated system in which the thrust line is tangent to the arch profile at the three hinges ($P_1^0(x_1^0, y_1^0)$, $P_2^0(x_2^0, y_2^0)$ and $P_3^0(x_3^0, y_3^0)$) associated to the mechanism. The Equation (4) of virtual works, taking into account the assumption (5), becomes

$$\left\langle g, \delta^{0*} \right\rangle + R_0^0 \cdot \delta_0^{0*} = 0 \tag{12}$$

so that the reaction force is obtained by

$$R_0^0 = -\frac{\left\langle g, \delta^{0*} \right\rangle}{\delta_0^{0*}} \tag{13}$$

Given the hinges position in the initial configuration Ω^0, it is possible to study the settled configuration Ω^k (second step) characterized by a settlement $\delta_0^k(u_0^k, v_0^k)$, applied at $P_0(x_0, y_0)$, which components are

$$u_0^k = \delta_0^k \cos\theta \tag{14}$$

$$v_0^k = \delta_0^k \sin\theta \tag{15}$$

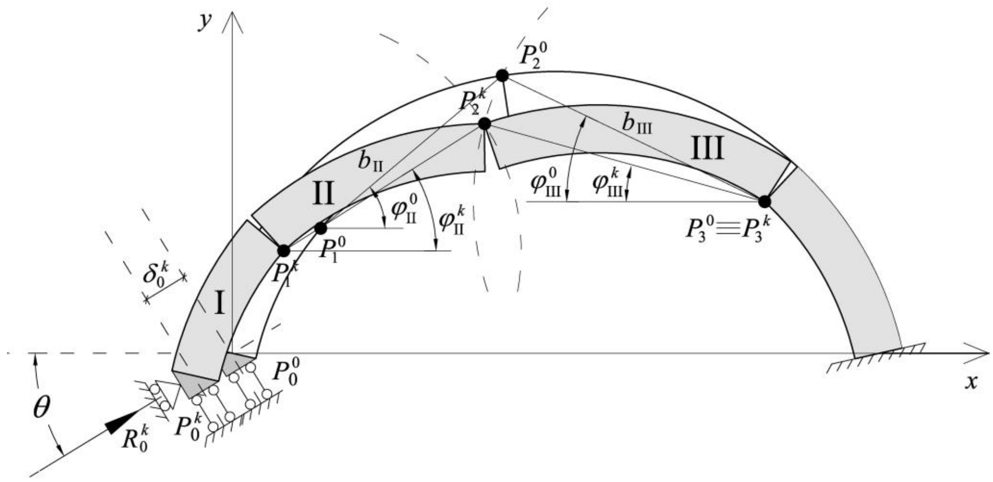

Figure 3. Graphical representation of the kinematic mechanism in the generic settled configuration Ω^k.

Also in this step, the right mechanism in the Ω^k configuration, resulting by the application of the settlement $\delta_0^k(u_0^k, v_0^k)$, is reached through an iterative procedure, assuring the validity of Heyman's conditions. In fact, the position of the hinges $P_1^k(x_1^k, y_1^k)$, $P_2^k(x_2^k, y_2^k)$ and $P_3^k(x_3^k, y_3^k)$ may not coincide with P_1^0, P_2^0 and P_3^0 of Ω^0, due to the possible occurrence of the change mechanism phenomenon previously described.

The mechanism, illustrated in Figure 3, is defined by the motion of three hinged bodies, namely I, II and III, in the finite displacements field resulting by the assigned settlement $\delta_0^k(u_0^k, v_0^k)$. The rotational parameters $\left(\varphi_{\mathrm{II}}^0, \varphi_{\mathrm{III}}^0\right)$ and $\left(\varphi_{\mathrm{II}}^k, \varphi_{\mathrm{III}}^k\right)$ – which identify the placement of the body II and III in the unsettled Ω^0 and settled Ω^k configuration respectively – are related to the settlement components through the following relations

$$u_0^k = u_1^k = x_1^k - x_1^0 = b_{\mathrm{II}}^0 \cos\varphi_{\mathrm{II}}^0 + b_{\mathrm{III}}^0 \cos\varphi_{\mathrm{III}}^0 - b_{\mathrm{II}}^k \cos\varphi_{\mathrm{II}}^k - b_{\mathrm{III}}^k \cos\varphi_{\mathrm{III}}^k \tag{16}$$

$$v_0^k = v_1^k = y_1^k - y_1^0 = -b_{\mathrm{II}}^k \sin\varphi_{\mathrm{II}}^k + b_{\mathrm{III}}^k \sin\varphi_{\mathrm{III}}^k \tag{17}$$

where b_{II} and b_{III} are the distances $\overline{P_1P_2}$ and $\overline{P_2P_3}$ respectively, evaluated both in the unsettled or settled configuration.

The Equations (15) and (14) lead to the expressions of the rotational parameters $\left(\varphi_{\mathrm{II}}^k, \varphi_{\mathrm{III}}^k\right)$ evaluated in the deformed configuration

$$\varphi_{\mathrm{II}}^k = \arcsin\left[\frac{1}{b_{\mathrm{II}}^k}\left(b_{\mathrm{III}}^k \sin\varphi_{\mathrm{III}}^k - \delta^k \sin\theta\right)\right] \tag{18}$$

$$\varphi_{\mathrm{III}}^k = \arccos\left[\frac{1}{b_{\mathrm{III}}^k}\left(b_{\mathrm{II}}^0 \cos\varphi_{\mathrm{II}}^0 + b_{\mathrm{III}}^0 \cos\varphi_{\mathrm{III}}^0 - b_{\mathrm{II}}^k \cos\varphi_{\mathrm{II}}^k - \delta_0^k \cos\theta\right)\right] \tag{19}$$

The incremental values of the rotational parameters $\left(\Delta\varphi_{\mathrm{II}}^k, \Delta\varphi_{\mathrm{III}}^k\right)$ associated to the passage from the unsettled Ω^0 and settled Ω^k configurations are directly obtained by the relations

$$\Delta\varphi_{\mathrm{II}}^k = \varphi_{\mathrm{II}}^0 - \varphi_{\mathrm{II}}^k \tag{20}$$

$$\Delta\varphi_{\mathrm{III}}^k = \varphi_{\mathrm{III}}^0 - \varphi_{\mathrm{III}}^k \tag{21}$$

Given the above Equations (14)-(21), the displacement components of each point of the arch in the settled configuration can be obtained. With reference to the body I, the horizontal and vertical components, u_i^k and v_i^k respectively, of the displacement vector at a generic point $Q^k(x_i^k, y_i^k)$ are

$$u_i^k = u_0^k = \delta_0^k \cos\theta \tag{22}$$

$$v_i^k = v_0^k = \delta_0^k \sin\theta \tag{23}$$

Concerning with the body II, the displacement components in the case of $x_i^k > x_1^0$ are

$$u_i^k = u_0^k - \sqrt{\left(x_1^0 - x_i^k\right)^2 + \left(y_1^0 - y_i^k\right)^2}\cos\Delta\varphi_{\mathrm{II}}^k \tag{24}$$

$$v_i^k = v_0^k - \sqrt{\left(x_1^0 - x_i^k\right)^2 + \left(y_1^0 - y_i^k\right)^2}\sin\Delta\varphi_{\mathrm{II}}^k \tag{25}$$

while in the case of $x_i^k < x_1^0$ are

$$u_i^k = u_0^k + \sqrt{\left(x_1^0 - x_i^k\right)^2 + \left(y_1^0 - y_i^k\right)^2}\cos\Delta\varphi_{\mathrm{II}}^k \tag{26}$$

$$v_i^k = v_0^k + \sqrt{\left(x_1^0 - x_i^k\right)^2 + \left(y_1^0 - y_i^k\right)^2}\sin\Delta\varphi_{\mathrm{II}}^k \tag{27}$$

As far as it concerns the body III, the following relations are given for the case of $x_i^k < x_3^0$

$$u_i^k = \sqrt{\left(x_3^0 - x_i^k\right)^2 + \left(y_3^0 - y_i^k\right)^2}\cos\Delta\varphi_{\mathrm{II}}^k \tag{28}$$

$$v_i^k = \sqrt{\left(x_3^0 - x_i^k\right)^2 + \left(y_3^0 - y_i^k\right)^2}\sin\Delta\varphi_{\mathrm{II}}^k \tag{29}$$

and for the case of $x_i^k > x_3^0$

$$u_i^k = -\sqrt{\left(x_3^0 - x_i^k\right)^2 + \left(y_3^0 - y_i^k\right)^2}\cos\Delta\varphi_{\mathrm{II}}^k \tag{30}$$

$$v_i^k = -\sqrt{\left(x_3^0 - x_i^k\right)^2 + \left(y_3^0 - y_i^k\right)^2}\sin\Delta\varphi_{\mathrm{II}}^k \tag{31}$$

After the kinematic definition of the configuration Ω^k, the third step of the procedure leads to the value of the reaction force R_0^k at the spreading support along θ direction through the Equation (6) and to the solution of the equilibrium problem (11). If the equilibrated system is statically admissible and the thrust line is everywhere inside the arch profile of each block passing through the hinges, is possible to increase the settlement to study the new configuration Ω^{k+1}. Otherwise is necessary to move the hinges, achieving the solution through few iterations in the configuration Ω^k before passing to the new configuration Ω^{k+1}.

Finally, the collapse condition, and then the ultimate admissible settlement, is reached with the occurrence of a kinematic chain which activates a mechanism.

3. Modelling of geometrical uncertainties with a probabilistic approach

3.1 Description of the random geometry

The analysis of masonry structures are generally affected by uncertainties due to both the geometrical irregularities and the variability of the materials mechanical properties. In this work, having the material infinite compressive strength and no-tensile property, only the effects of the geometrical irregularities are taken into account, following the probabilistic approach introduced by Cavalagli *et al*. [30]. Dealing with masonry arches, the geometrical uncertainties may be due to several causes: irregularities in the fabrication of the blocks (bricks and/or stones); imperfections due to the construction of both the arch and of the provisional structures placed for the supporting of the arch itself; irregularities related to the degradation of the materials over time. The geometrical irregularities of the arch has been modelled by means of a statistical approach, with the introduction of uncertain geometrical parameters. Such uncertainties are introduced with the aim to represent the geometrical irregularities that are generally unknown, in order to describe the different structural behaviour of arches having the same nominal geometry.

The following hypotheses are considered: random values of the angle of embrace α_i, the thickness t_i and the radius r_i of each voussoir, and deterministic value of the angle of embrace α (Figure 4). It should be noted that in this work the joint direction is not considered as random parameter, so that each joint of the random arch has a radial direction. The random parameters are defined by independent uniform probability density functions in a range of variability limited by a dimensional tolerance value ε as follows:

$$
\begin{aligned}
\alpha_i &= E[\alpha_i] + \varepsilon\,\alpha / n \cdot p_{\alpha_i} = \alpha / n + \varepsilon\,\alpha / n \cdot p_{\alpha_i} = \alpha / n\left(1 + \varepsilon\, p_{\alpha_i}\right) \\
\tilde{t}_i &= E[\tilde{t}_i] + \varepsilon\, t \cdot p_{t_i} = t + \varepsilon\, t \cdot p_{t_i} = t\left(1 + \varepsilon t\, p_{t_i}\right) \\
\tilde{r}_i &= E[\tilde{r}_i] + \chi\, r \cdot p_{r_i} = r + \chi\, r \cdot p_{r_i} = r\left(1 + \chi\, p_{r_i}\right)
\end{aligned}
\tag{32}
$$

where n is the number of voussoirs, χ is a curvature tolerance related to ε as $\chi = \varepsilon(t/r)$ and p_{α_i}, p_{t_i}, p_{r_i} are independent samples taken from a uniform probability density function in the range [-1,1] (Figure 5). The Equations (32) show that the mean values $E[\tilde{\bullet}]$ of the random geometrical parameters are assumed equal to the nominal values. Concerning the variable parts, the number of extracted samples are n for the random parameters $\tilde{t}_i$ and $\tilde{r}_i$, and $n-1$ for α_i in order to assure the deterministic value of the angle of embrace of the arch; the nth value of the sample results from the difference

$$
\alpha_n = \alpha - \sum_{i=1}^{n-1} \alpha_i \tag{33}
$$

The random nature of the geometrical parameters affects the description of the Cartesian coordinates of a generic point belonging to the arch. As an example, the Equations (2) and (3) indicating the centre of mass of the generic ith voussoir become

$$
\tilde{x}_i = r\cos\beta - \tilde{r}_i \cos\left(\beta + \frac{\tilde{\alpha}_i}{2}\right) \tag{34}
$$

$$
\tilde{y}_i = -r\sin\beta + \tilde{r}_i \sin\left(\beta + \frac{\tilde{\alpha}_i}{2}\right) \tag{35}
$$

for $i = 1$, and

$$
\tilde{x}_i = r\cos\beta - \tilde{r}_i \cos\left(\beta + \frac{\tilde{\alpha}_i}{2} + \sum_{m=1}^{i-1} \tilde{\alpha}_m\right) \tag{36}
$$

$$\tilde{y}_i = -r\sin\beta + \tilde{r}_i \sin\left(\beta + \frac{\tilde{\alpha}_i}{2} + \sum_{m=1}^{i-1}\tilde{\alpha}_m\right) \tag{37}$$

for $2 \le i \le n$.

In the analysis of the results, the probabilistic approach considers the mean values of loads and/or displacements, obtained at collapse, evaluated over a total number *h* of randomly generated cases equal to 1000 of each sample $\left(\alpha_i\right)_n^h$, $\left(\tilde{t}_i\right)_n^h$ and $\left(\tilde{r}_i\right)_n^h$, for a fixed number of voussoirs *n*. In [30] it has been already demonstrated that the introduction of geometrical uncertainties in the model affects the bearing capacity of an arch, obtaining lower values of the mean collapse loads with respect to the nominal values provided by a deterministic geometry. This aspect is related to the variability of the effective contact length between the voussoirs, which directly affects the strength criterion by limiting the position of the thrust line. In this paper this effect is taken into account in the kinematic description of the problem, developed in the finite displacement field, which considers the possible occurrence of the hinges at the extreme points of each effective contact length.

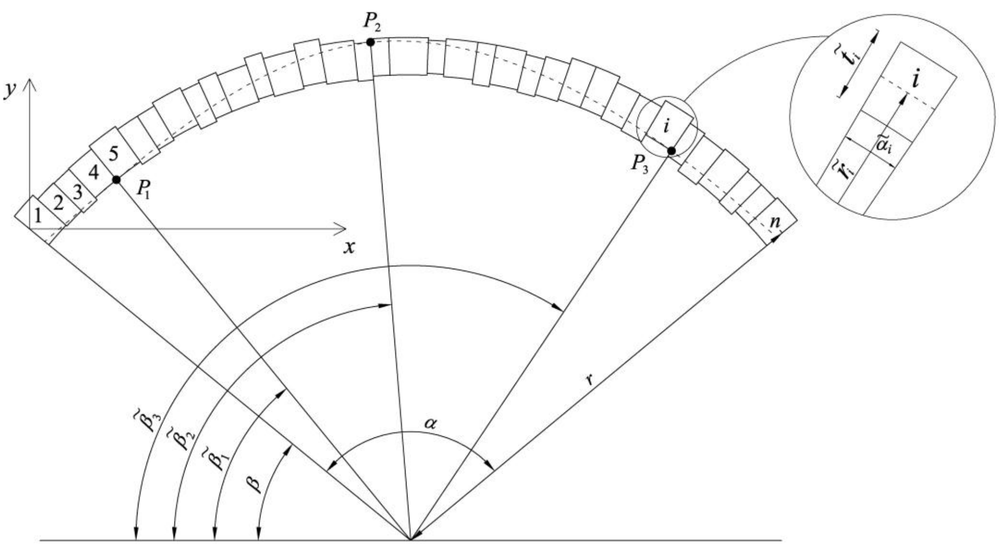

Figure 4. Masonry arch with geometrical irregularities described by the random values of the angle of embrace $\tilde{\alpha}_i$, the thickness $\tilde{t}_i$ and the radius $\tilde{r}_i$ of the *i*th voussoir.

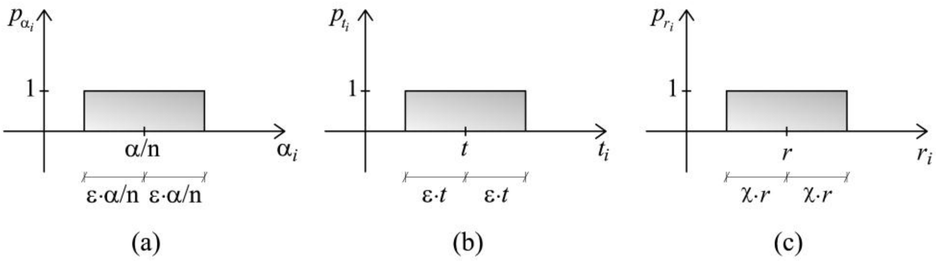

Figure 5. Probability density functions for the angle of embrace $\tilde{\alpha}_i$ (a), the thickness $\tilde{t}_i$ (b) and the radius $\tilde{r}_i$ (c).

3.2 A parametric investigation about the random effect

This Section reports the results of a parametric analysis of an arch subjected to a spreading support δ on a direction having an inclination $\theta = 45°$ on the horizontal (see Figure 2). The arch has the following nominal geometrical parameters: angle of embrace $\alpha = 102.78°$, radius $r = 1.40$ m and thickness $t = 0.12$ m, from which derived a dimensionless ratio $t/r = 0.08545$. The specific nominal geometry refers to a real masonry arch, which has been tested in the laboratory and described more in detail in the Section 4.2. The parametric analysis exposed in the following aims at investigating the uncertainties effects on the ultimate displacement to be expected in the experimental test. Following the probabilistic approach described in the previous Section, the geometrical irregularities of the voussoirs are considered assuming parameter $\varepsilon = 0.03$, due to the intrinsic values of tolerance affecting the bricks of the actual specimen [30]. Moreover, the effect of stereotomy is also taken into account by assuming several values of the number *n* of voussoirs in the range of 10 to 50. Following the approach previously described, for each value of *n*, 1000 samples of arches affected by geometrical uncertainties have been obtained.

The results, expressed in terms of the random variable $\left(\tilde{\delta}_u\right)_n^h$, has been interpolated through the normal probability density function

$$p_{\tilde{\delta}_u} = f\left(\tilde{\delta}_u \mid \mu, \sigma\right) = \frac{1}{\sigma\sqrt{2\pi}} \mathrm{e}^{\frac{-\left(\tilde{\delta}_u - \mu\right)^2}{2\sigma^2}} \tag{38}$$

where $\mu = E[\tilde{\delta}_u]$ and $\sigma^2 = \sigma^2[\tilde{\delta}_u] = E[\tilde{\delta}_u - \mu]^2$ are the mean value and the variance of the sample of the random ultimate displacement (Figure 6). It is worth noting as the spread and the mean values of the ultimate displacement decrease with the increase of the number of the voussoirs. Furthermore, for each fixed value of *n*, the mean final displacement is always lower than the displacement value obtained by using the nominal geometry. Table 1 summarizes the results. It should be also noted that, for the arch geometry in exam, as the displacement δ_k of the settled springing increases, the position $\tilde{\beta}_j$ of the cracking hinges changes. This change occurs at between 80% and 90% of the final displacement, as shown by the graph in Figure 7, which represents, for the case of *n*=50, the value of the position of the hinges in the model with nominal geometry and the mean value of the random position of the hinges $\left(\tilde{\beta}_j - \beta\right)$ obtained in the model with irregular geometry, both normalized with respect to the angle of embrace α. The graph highlights that, for the case of *n*=50, the mean position of the hinges obtained by probabilistic analysis on the irregular geometry is quite close to the position obtained from deterministic analysis. Figure 8 shows the position of the hinges, as a function of *n,* in the initial configuration (Figure 8a) and in the final configuration (Figure 8b), in which can be observed a higher uncertainty in the definition of the cracking hinges for a low number *n* of voussoirs. However, in terms of mean values, the position of hinges 1, 2 and 3 differs slightly from the value obtained from deterministic analysis.

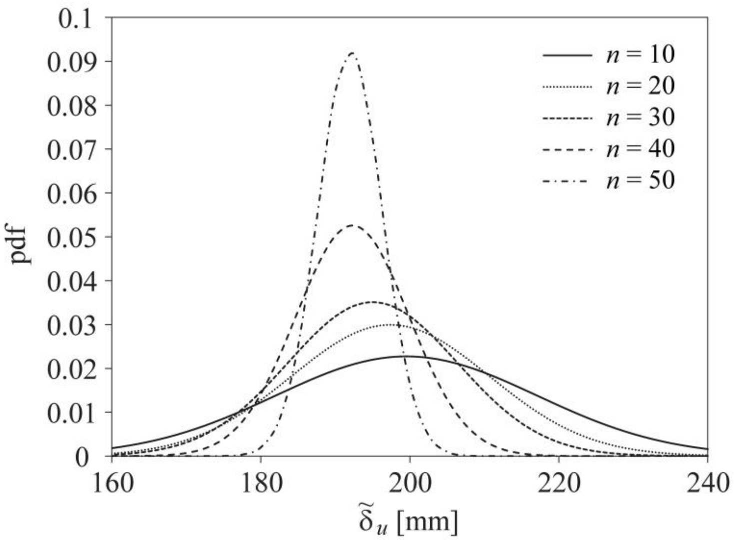

Figure 6. Probability density function of the random ultimate displacement for arches at different values of the number *n* of voussoirs (*n* equal to 10, 20, 30, 40 and 50).

Table 1. Ultimate displacements obtained by numerical analysis at different values of the number n of voussoirs (*n* equal to 10, 20, 30, 40 and 50) using nominal and irregular geometry.

Nominal geometry		Irregular geometry	
δ_u [mm]	n	μ [mm]	σ [mm]
234.10	10	199.54	17.56
230.01	20	197.41	13.33
226.04	30	195.02	11.37
222.00	40	192.31	7.59
217.90	50	191.99	4.32

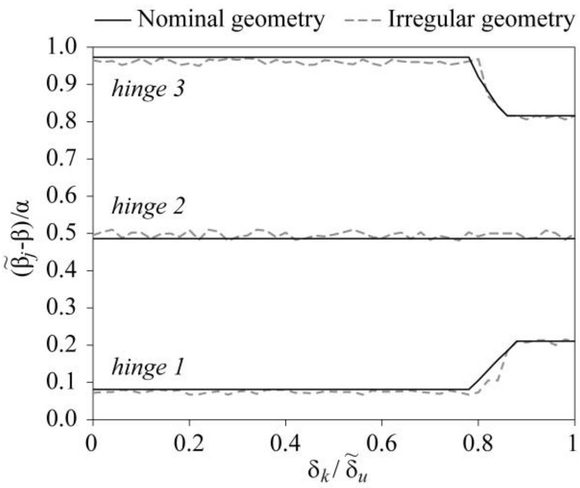

Figure 7. Evolution of the normalized position $\left[\left(\tilde{\beta}_j-\beta\right)/\alpha\right]$ of hinges 1, 2 and 3 in function of the normalized settlement $(\delta_k/\tilde{\delta}_u)$ at the springing, for the case of nominal (continuous lines) and irregular (dashed lines) geometry, evaluated in average.

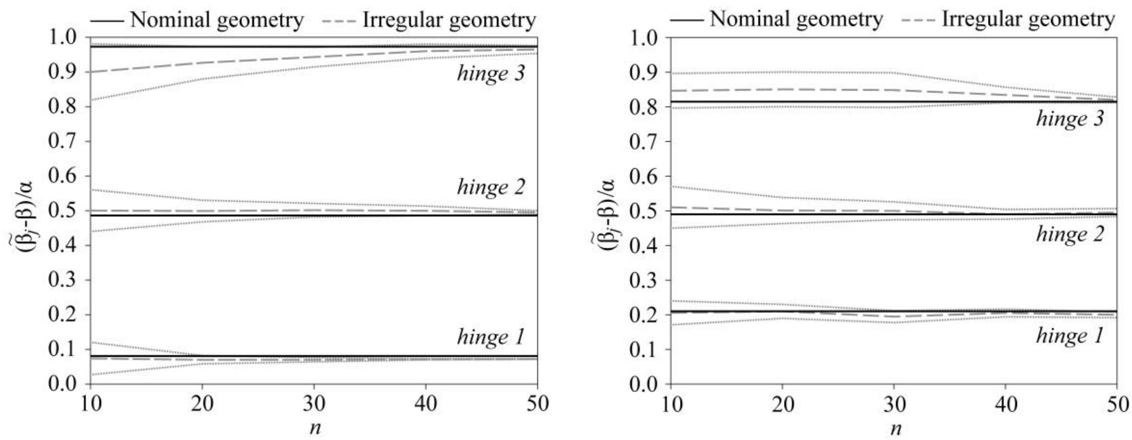

(a) (b)

Figure 8. Normalized position $\left[\left(\tilde{\beta}_j-\beta\right)/\alpha\right]$ of hinges 1, 2 and 3 in function of the number *n* of voussoirs, for the case of nominal (continuous lines) and irregular (dashed lines) geometry, in the initial (a) and ultimate (b) configuration. The dotted lines below and above the continuous curve are related to the values μ-σ and μ+σ respectively.

4. Experimental tests

In this section, the comparison between the results obtained by proposed numerical procedure and two related experimental tests is reported. The first refers to a round arch subjected to horizontal settlement developed by Ochsendorf [33]; in the second, a springing of a segmental arch has been subjected to incremental settlements along a direction inclined of 45° angle from the horizontal (Figure 2).

4.1 Horizontal spreading support

The small-scale experimental test carried out by Ochsendorf [33] considered as a case of study refers to an arch comprising 16 concrete blocks (Figure 9a), with a 50 mm radial thickness, mean radius *r* of 220 mm and thickness-radius ratio $t/r = 0.23$.

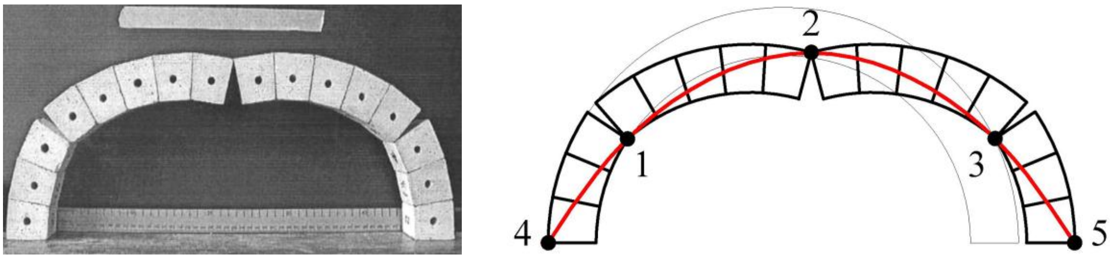

(a) (b)

Figure 9. (a) Experimental test carried out by Ochsendorf [33]: equilibrium state of a settled configuration before collapse. (b) Theoretical symmetric five-hinges collapse mechanism.

On this arch, a springing was subjected to incremental horizontal settlement until reaching the final condition. Experimental testing showed that the cracking hinges (1, 2 and 3) do not change in position from the initial to the final condition. Furthermore, the maximum measured displacement (30 mm) was reached with an increment of 15.4% of the span with respect to the internal radius (Figure 9b). In Figure 9a the instant immediately before the collapse is shown. From this instant on, the arch has lost its stability and the collapse occurred with a pure rotational mechanism. An important observation made by Ochsendorf was that the expected theoretical five-hinges mechanism did not occur owing to model imperfections, which reduced the ultimate displacement δ_u at springing from the predicted value of about 33 mm to 30 mm. The theoretical collapse condition was obtained through the study of the limit equilibrium, which is commonly used considering the nominal arch geometry. In general, the results quite accurately represents both the arch configurations and the position at which the hinges occur (Figure 10), nonetheless, an error of the final displacement estimation, which in some cases may not be neglected, could be done. The same results of Ochsendorf's analyses are obtained by Coccia *et al.* [35], in which the problem of the right ultimate displacement estimation is highlighted, making the focus on the geometric imperfections that are found in the real arch.

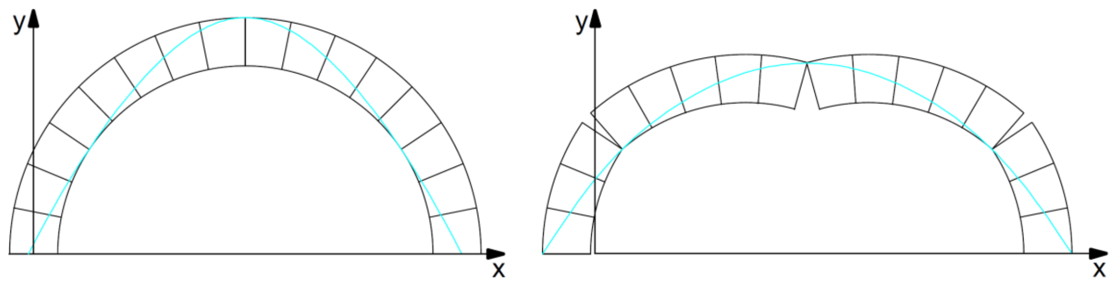

(a) (b)

Figure 10. Masonry arch with nominal geometry: thrust line in the initial (a) and ultimate (b) configuration.

In this work, an interpretation of the experimental observation has been provided by introducing geometrical uncertainties in the model through the probabilistic approach described in Section 3. Fixing the number of the voussoirs (n=16), 1000 samples of arches affected by geometrical uncertainties have been generated. The random parameters have been generated using the Equations (32) and setting three levels of tolerance ε (0.01, 0.02 and 0.03). Figure 11 shows the case of a random arch, with ε =0.03, in the initial state characterized by the three-hinges chain. The geometrical irregularities determine the natural loss of symmetry in the mechanism, so that the ultimate condition is reached, by increasing the displacement of a springing, with the occurrence of a fourth hinge at the extrados of the left or right springing alternatively.

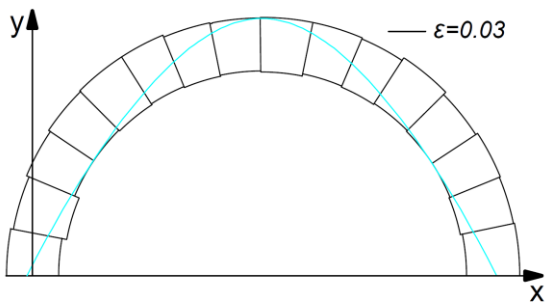

Figure 11. Masonry arch with irregular geometry (ε = 0.03): thrust line in the initial configuration.

In Figure 12 the histogram of the probability density of the random ultimate displacement $\tilde{\delta}_u$ has been represented for ε equal to 0.01, 0.02 and 0.03. Given the Skewness (Γ_S) and Kurtosis (Γ_K) values related to each population of $\left(\tilde{\delta}_u\right)^{\varepsilon}$, the normal probability density function $p_{\tilde{\delta}_u}$ expressed by the Equation (38) has been used to interpolate in first approximation the numerical results.

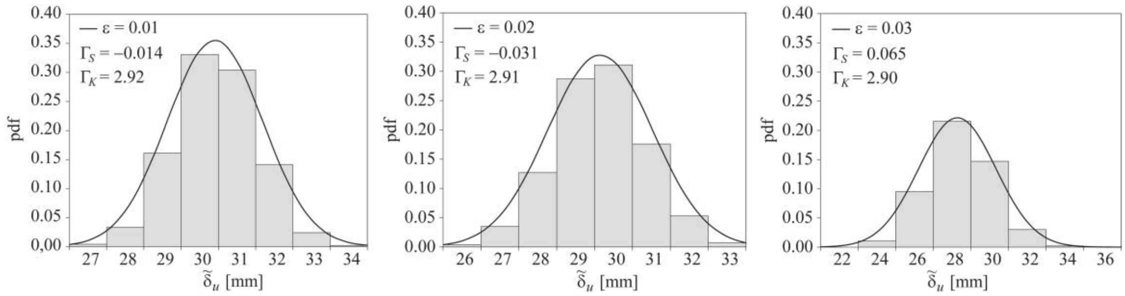

(a) (b) (c)

Figure 12. Histogram of the probability density of the ultimate displacement $\left(\tilde{\delta}_u\right)^{\varepsilon}$, with its interpolant normal probability density function, for the case of ε equal to 0.01 (a), 0.02 (b) and 0.03 (c).

The normal distributions of Figure 12 have been superimposed with the experimental and numerical results performed using nominal geometry (Figure 13). The graph highlights that the greater the level of tolerance ε, the greater the spread of the interpolant normal distribution and the lower the mean value of the random ultimate displacement. It is interesting to note that the probabilistic approach provides a more consistent prediction of the experimental displacement observed by Ochsendorf, considering a value of ε between 0.01 and 0.02. Table 2 summarizes the comparison between the experimental observations and the numerical results obtained using nominal geometry and the probabilistic approach, with reference to the mean and standard deviation values. Finally, it is conceivable to consider that the deviation between the results obtained by the experimental tests and by numerical simulation with nominal geometry can be related to uncertainties in the actual geometry of the arch.

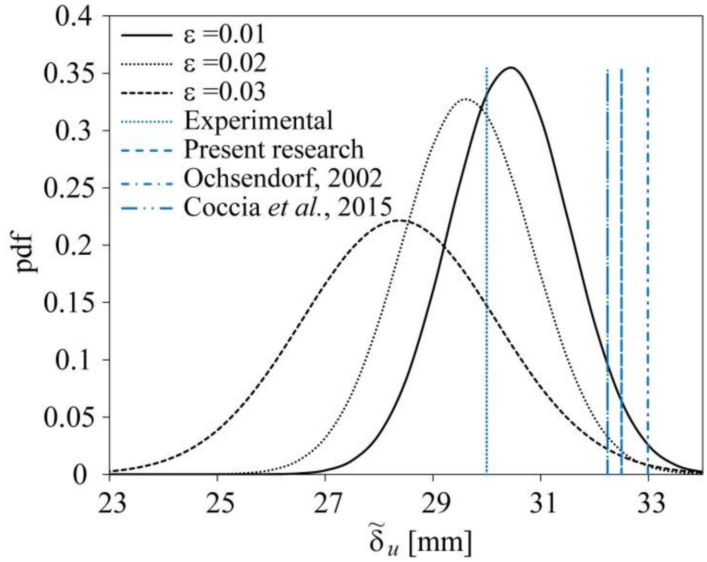

Figure 13. Comparison between the ultimate displacement values obtained by the experimental test, by numerical analysis using nominal geometry and the normal distributions of the random ultimate displacement values given by the probabilistic approach (ε equal to 0.01, 0.02 and 0.03).

Table 1. Ultimate displacements obtained by experimental test and numerical analysis using nominal and irregular geometry.

Experimental test	Numerical analysis				
Real geometry	Nominal geometry		Irregular geometry		
δ_u [mm]	Reference	δ_u [mm]	ε	μ [mm]	σ [mm]
	Ochsendorf, 2002	32.9	0.01	30.42	1.1
30.0	Coccia *et al.*, 2015	32.2	0.02	29.63	1.2
	Present research	32.5	0.03	28.37	1.8

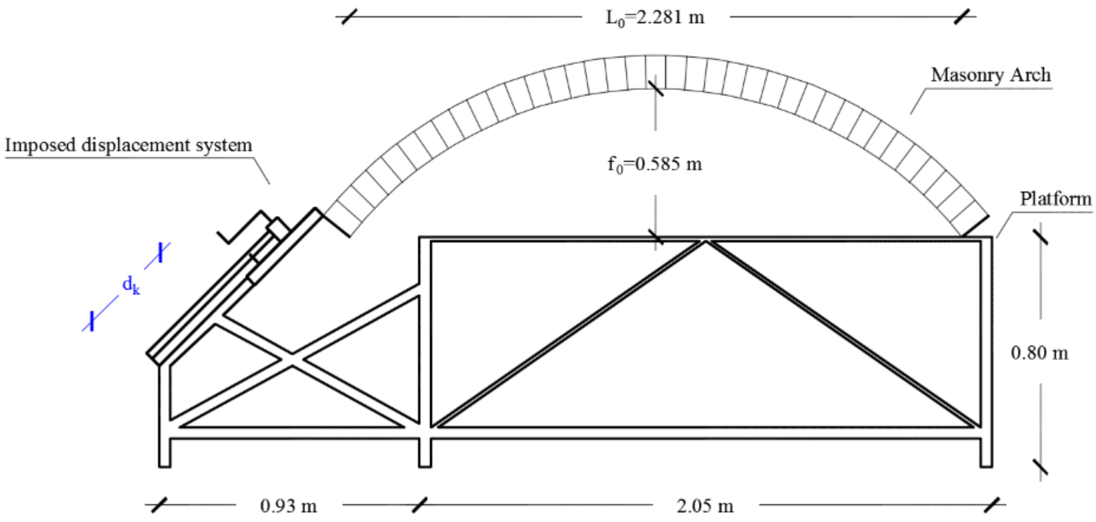

Figure 14. Specimen geometry and test layout.

4.2 No-horizontal spreading support

The masonry arch described in Section 3.2 refers to a real structure constructed and tested in the laboratory. The arch has a nominal span of 2.281 m, a nominal net rise of 0.585 m and is constituted by 37 bricks assembled with mortar joints (Figure 14). The arch complies with Heyman's condition of zero resistance between the interfaces of the blocks, as a Plexiglas plate was inserted (Figure 15a) in the middle of each mortar joint. For this reason, mortar hinges formed at the interface between the Plexiglas plate and the mortar (Figure 15b). The structure is placed on a steel frame system featuring a moveable springing (left springing) along a direction inclined of 45° with respect to the horizontal. The test system provides an instant-by-instant displacement measurement, until the structural collapse. The support movement has been imposed with a manual system, and the displacement measured with an LVDT activated simultaneously with a video recording of the test. The collapse condition occurred with a three-hinges mechanism in correspondence to an ultimate displacement of about 195 mm (Figure 15c).

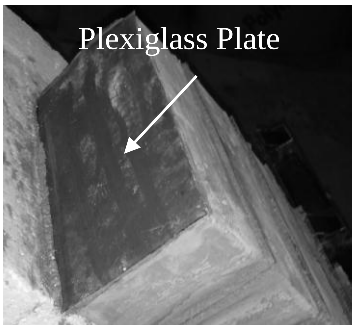

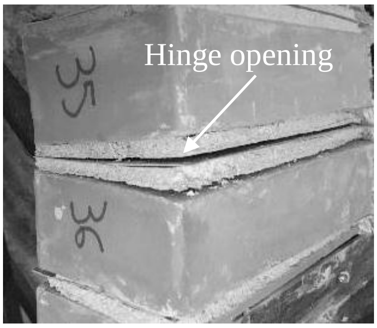

(a) (b)

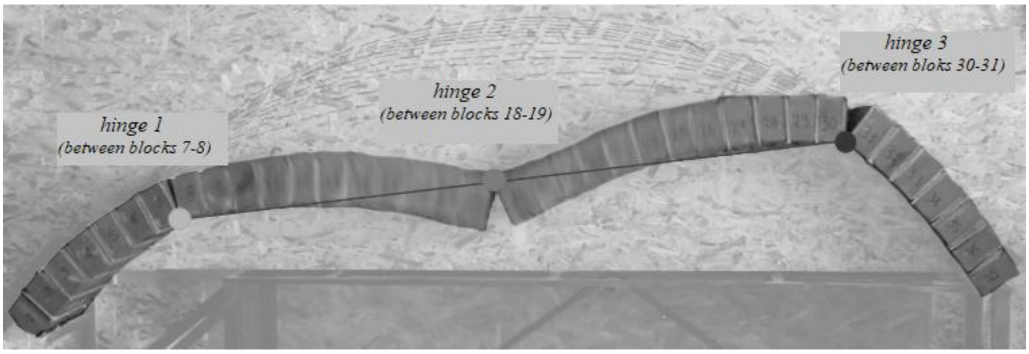

(c)

Figure 15. (a) Plexiglas plate inserted in the middle of the mortar joint. (b) Opening of the hinge corresponding to the Plexiglas plates (initial hinge configuration). (c) Arch collapse condition.

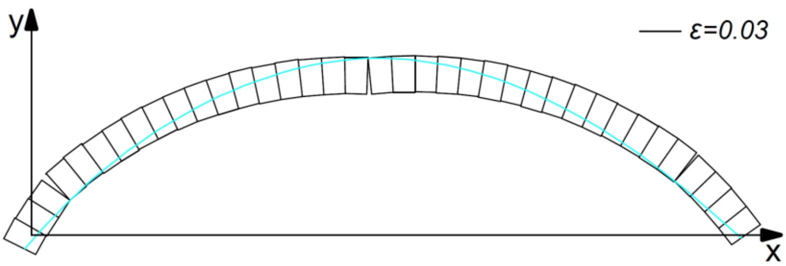

Figure 16. A case extracted from random arch samples with a tolerance value $\varepsilon = 0.03$ in an equilibrated settled configuration Ω^k ($\tilde{\delta}_k = 69.6$ mm).

The numerical procedure proposed in this paper has been used to simulate the experimental test, both with nominal and irregular geometry ($\varepsilon = 0.03$) using the probabilistic approach. In Figure 16 a case extracted from random arch samples is illustrated in an equilibrated settled configuration Ω^k.

Fixing the number of voussoirs (n=37), 1000 samples have been generated considering $\left(\alpha_i\right)^h$, $\left(\tilde{t}_i\right)^h$ and $\left(\tilde{r}_i\right)^h$ as random geometrical parameters and analysed through the proposed procedure. As expected from the parametric analysis carried out in Section 3.2, the configuration of hinges 1, 2 and 3 changes with the increase of the displacement δ_k imposed to the left springing. The proposed algorithm, by updating the position of the hinges via the thrust line, is able to accurately represent this phenomenon of change in hinge position throughout the development of the mechanism up to the collapse, as can be seen from the graph in Figure 17. The figure shows the evolution of the normalized hinge position $\left[\left(\tilde{\beta}_j - \beta\right)/\alpha\right]$ in function of the normalized settlement at the springing $(\delta_k / \tilde{\delta}_u)$ obtained during the experimental test (Figure 17a) and by numerical simulations (Figure 17b).The localizations of hinges 1, 2 given by numerical analysis are quite similar to those observed in the experimental test, while the position of hinge 3 are quite different. However, it must be considered that the results reported in Figure 17b are evaluated as a mean over 1000 samples, thus the presence of consistent solutions cannot be a priori excluded. In Figure 18 the results in terms of ultimate displacement are shown.

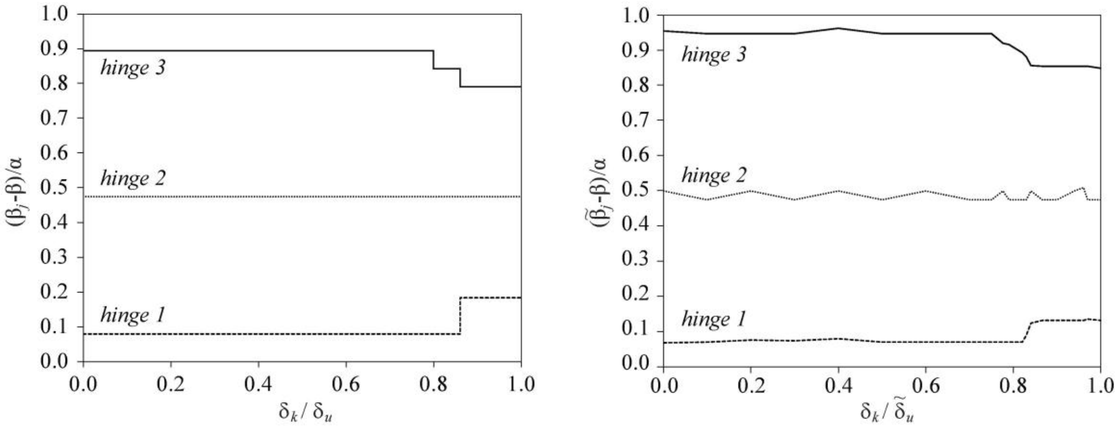

(a) (b)

Figure 17. Evolution of the normalized position $\left[\left(\tilde{\beta}_j-\beta\right)/\alpha\right]$ of hinges 1, 2 and 3 in function of the normalized settlement $(\delta_k/\tilde{\delta}_u)$ at the springing. (a) Results of experimental test. (b) Mean values provided by the numerical simulations based on the probabilistic approach.

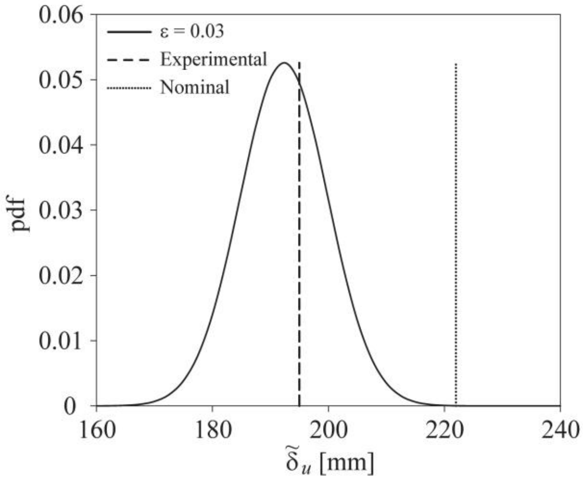

Figure 18. Comparison between probabilistic results (continuous curve), numerical simulations with nominal arch geometry (dotted line) and experimental results (dashed line).

The normal distribution which interpolates the obtained random ultimate displacement are plotted in Figure 18 with the deterministic values obtained by the experimental test and the numerical simulation carried out considering the nominal geometry. The graph highlights that, in average, the results given by irregular geometry (mean value of about 192.5 mm) provide a more consistent prediction of the experimental ultimate displacement (195 mm) than the case of nominal geometry (222 mm), reducing the error from 13.8% to 1.3%.

Finally, it has been demonstrated that the overestimations of the collapse condition, in terms of both displacements and reaction forces, generally observed by the direct application of the limit equilibrium approach on structures having nominal geometry, with respect to the experimental observations, can be corrected by introducing uncertainties in the model. More in general, depending on the specific structure in exam and on its geometrical irregularities with respect to the actual geometry, an investigation about the influence of the uncertainties on the ultimate condition should be carried out with a probabilistic approach. Then, a safety factor evaluated as the ratio

$$\gamma_s = \frac{E[\tilde{\Psi}] - \sigma[\tilde{\Psi}]}{\Psi_{nom}}$$

where $\tilde{\Psi}$ is the considered random variable (collapse load, ultimate displacement, etc.) and Ψ_{nom} its deterministic value obtained by using a nominal geometry, returns the amount of error that could affect the analysis if the irregular geometry is not taken into account. For the interested reader, an example of application of such a procedure to the masonry arch can be found in [30].

5. Conclusions

In this paper, the behaviour of the masonry arch on no-horizontal spreading supports has been analysed, taking into account the geometrical irregularities effects. A numerical procedure based on the limit equilibrium approach has been developed in large displacements field, in order to follow the evolution of the mechanism until the collapse with the incremental increase of the imposed settlement. The algorithm makes use of the Principle of Virtual Work to solve static problem, and it is able to reach the collapse conditions characterized by all the mechanisms described above. The geometrical irregularities have been considered as intrinsic uncertainties of the structures and spread on the arch model by means of three random variables. These random parameters, namely the radius of curvature, the thickness and the angle of embrace of each voussoir, have been described through independent uniform probability density functions. It should be noted that each type of random structural analysis, is a result of a significant number of samples analysed in a probabilistic sense.

The procedure has been applied to two experimental tests. The former is the well-known test carried out by Ochsendorf concerning a semi-circular arch made by 16 blocks subjected to horizontal settlements at both the supports. The numerical simulations of the test, provided by Ochsendorf himself and recently by Coccia and co-authors, show a little overestimation of the ultimate admissible displacement with respect to the experimental observations. In this paper has been demonstrated that the overestimation (about 6.8%) of the ultimate condition obtained by a structure with nominal geometry could be corrected by including uncertainties in the model. In particular, it has been shown that considering an error between 1% and 2% of the dimensions of the blocks, the experimental results could be better reproduced. The latter test refers to a segmental arch, made of 37 bricks, on a springing support with an inclination of 45° on the horizontal. Also in this case the numerical simulations carried out on the nominal geometry has provided an overestimation of the ultimate displacement (about 13.8%) with respect to the experimental results, while including the geometrical uncertainties in the model with an error of 3% of the brick dimensions a more consistent estimation of the actual structural capacity can be achieved.

Finally, the obtained results highlight that the uncertainties effects cannot be neglected in the performance evaluations of experimental tests and, even more, this aspect should be considered more in general in structural analysis. The role of uncertainties will be as significant as the level of structural and/or material degradation will be. The choice of the tolerance level, which describes the irregularities in the statistical model, determines the quality of the results and must be defined in function of the case in exam. In this context, geometrical safety factors could be introduced, in order to take into account the uncertainties effects on the analysis of actual structures.

Acknowledgments

The Authors gratefully acknowledge support from the Italian Ministry of Education, University and Scientific Research, within the PRIN National Grant 2015 project ‘‘Advanced mechanical modeling of new materials and structures for the solution of 2020 Horizon challenges’’ (Prot. 2015JW9NJT).

References

[1] Heyman J, The stone skeleton. International Journal of Solids and Structures, 1966; 2:249-279.

[2] Heyman J. The safety of masonry arches. Int J Mech Sci 1969; 11:363-85.

[3] Heyman J. Why ancient cathedrals stand up: the structural design of masonry, Ingenia 2001; 10:19.23.

[4] Romano A, Ochsendorf JA, The mechanics of gothic masonry arches, Int J Archit Herit 4(1) (2010) 59-82.

[5] Cocchetti G, Colasante G, Rizzi E. On the analysis of minimum thickness in circular masonry arches. Appl Mech Rev 2011;64(5):051002.1–051002.22.

[6] Makris N, Alexakis H. The effect of stereotomy on the shape of the thrust-line and the minimum thickness of semicircular masonry arches. Arch Appl Mech 2013;83:1511–33.

[7] Alexakis H, Makris N. Limit equilibrium analysis and the minimum thickness of circular masonry arches to withstand lateral inertial loading. Arch Appl Mech 2014;84:757–72.

[8] Dimitri R, Tornabene F. A parametric investigation of the seismic capacity for masonry arches and portals of different shapes. Eng Fail Anal 2015;52:1–34.

[9] Cavalagli N, Gusella V, Severini L. Lateral loads carrying capacity and minimum thickness of circular and pointed masonry arches, International Journal of Mechanical Sciences 2016; 115-116;645–656.

[10] Nikolić D. Thrust line analysis and the minimum thickness of pointed masonry arches, Acta Mechanica 2017; 228(6):2219-2236.

[11] Lengyel G. Minimum thickness of the gothic arch. Arch Appl Mech 2018; 88(5):769-788.

[12] Lengyel G. Discrete element analysis of gothic masonry vaults for self-weight and horizontal support displacement, Engineering Structures 2017; 148:195–209.

[13] Block P, Ochsendorf J. Thrust network analysis: A new methodology for three-dimensional equilibrium, Journal of the International Association for Shell and Spatial Structures 2007; 48(155):167-173.

[14] Fraternali F, A thrust network approach to the equilibrium problem of unreinforced masonry vaults via polyhedral stress functions, Mechanics Research Communications 2010; 37(2):198-204.

[15] Michiels T, Adriaenssens S, Form-finding algorithm for masonry arches subjected to in-plane earthquake loading, Computers and Structures 2018; 195:85–98.

[16] Tralli A, Alassandri C, Milani G, Computational methods for masonry vaults: a review of recent results. Open J. Civ. Eng 2014, 8(1):272-287.

[17] Sarhosis V, De Santis S, de Felice G, A review of experimental investigations and assessment methods for masonry arch bridges, Structure and Infrastructure Engineering 2016, 12(11):1439-1464.

[18] Chiozzi A, Malagu' M, Tralli A, Cazzani A, ArchNURBS: NURBS-Based Tool for the Structural Safety Assessment of Masonry Arches in MATLAB. Journal of Computing in Civil Engineering 2016, 30(2): Article number 04015010.

[19] Chiozzi A, Milani G, Tralli A, A Genetic Algorithm NURBS-based new approach for fast kinematic limit analysis of masonry vaults. Computers and Structures 2017, 182(1):187-204.

[20] Caporale L, Luciano R, Rosati L. Limit analysis of masonry arches with externally bonded FRP reinforcements. Comput Meth Appl Mech Eng 2006;196(1–3):247–60.

[21] Caporale A, Feo L, Hui D, Luciano R. Debonding of FRP in multi-span masonry arch structures via limit analysis. Compos Struct 2014;108:586–865.

[22] Grande E, Milani G. Modeling of FRP-strengthened curved masonry specimens and proposal of a simple design formula. Compos Struct 2016;158:281–90.

[23] Bertolesi E, Milani G, Fedele R, Fast and reliable non-linear heterogeneous FE approach for the analysis of FRP-reinforced masonry arches. Composites Part B: Engineering 2016, 80:189-200.

[24] Bertolesi E, Milani G, Carozzi FG, Poggi C. Ancient masonry arches and vaults strengthened with TRM and FRP composites: Numerical analyses, Composite Structures, 2018, 187:385-402.

[25] Alecci V, Focacci F, Rovero L, Stipo G, De Stefano M. Extrados strengthening of brick masonry arches with PBO–FRCM composites: Experimental and analytical investigations, Composite Structures 2016; 149:184–196.

[26] de Arteaga I., Morer P. The effect of geometry on the structural capacity of masonry arch bridges, Construction and Building Materials 2012; 34:97-106.

[27] Conde B., Díaz-Vilariño L., Lagüela S., Arias P. Structural analysis of Monforte de Lemos masonry arch bridge considering the influence of the geometry of the arches and fill material on the collapse load estimation, Construction and Building Materials 2016; 120:630–642.

[28] Zampieri P, Zanini M, Faleschini F. Influence of damage on the seismic failure analysis of masonry arches. Constr Build Mater 2016;119:343–55.

[29] Zanaz A, Yotte S, Fouchal F, Chateauneuf A. Efficient masonry vault inspection by monte carlo simulations: case of hidden defect. Case Stud Struct Eng 2016;5:1–12.

[30] Cavalagli N, Gusella V, Severini L. The safety of masonry arches with uncertain geometry, Computers and Structures 2017; 188:17-31.

[31] Severini L, Cavalagli N, DeJong M, Gusella V, Dynamic response of masonry arch with geometrical irregularities subjected to a pulse-type ground motion, Nonlinear Dynamics 2018; 91(1):609-624.

[32] Como M, On the role played by settlements in the statics of masonry structures, in: The conference on geotechnical engineering for the preservation of monuments and historic sites (ed. Viggiani), Balkema, Rotterdam, 1997, 81-87.

[33] Ochsendorf JA, The masonry arch on spreading supports, Struct Eng Inst Struct Eng Lond 2006; 84(2):29-36.

[34] Galassi S, Paradiso M, Tempesta G, Non-Linear Analysis of Masonry Structures Subjected to External Settlements, Open Journal of Civil Engineering 2013; 3:18-26.

[35] Coccia S, Di Carlo F, Rinaldi Z, Collapse displacements for a mechanism of spreading-induced supports in a masonry arch, International Journal of Advanced Structural Engineering 2015; 7(3):307-320.

[36] Zhang Y, Macorini L, Bassam A. Izzuddin, Numerical investigation of arches in brick-masonry bridges, Structure and Infrastructure Engineering 2017 (in press), DOI:10.1080/15732479.2017.1324883.

[37] Zampieri P, Zanini MA, Faleschini F, Hofer L, Pellegrino C, Failure analysis of masonry arch bridges subject to local pier scour, Engineering Failure Analysis 2017; 79:371-384

[38] Zampieri P, Faleschini F, Zanini MA, Simoncello N, Collapse mechanisms of masonry arches with settled springing, Engineering Structures 2018; 156:363-374

[39] Zampieri P, Simoncello N, Pellegrino C, Structural behaviour of masonry arch with no-horizontal springing settlement, Frattura ed Integrità Strutturale 2018; 12(43):182-190.

[40] Como M, Static of Historic Masonry Constructions, 3rd Edition, Springer International Publishing AG, 2017.